Experiment and modeling of the deposition of ultrananocrystalline diamond films using hot filament chemical vapor deposition and $Ar/CH_4/H_2$ gas mixtures: A generalized mechanism for ultrananocrystalline diamond growth

P. W. May[a)]
School of Chemistry, University of Bristol, Bristol BS8 1TS, United Kingdom

Yu. A. Mankelevich
Nuclear Physics Institute, Moscow State University, 119992 Moscow, Russia

(Received 10 February 2006; accepted 10 May 2006; published online 17 July 2006)

$Ar/CH_4/H_2$ gas mixtures have been used to deposit nanocrystalline diamond (NCD) and ultrananocrystalline diamond (UNCD) films using hot filament (HF) chemical vapor deposition. The $Ar:H_2$ concentration was maintained at $Ar/(H_2+Ar)=80\%$ while the CH_4 concentration was varied over the range $CH_4/(H_2+CH_4)=0.3-6.0$. For higher methane concentrations, the filament became coated in a graphitic layer which prevented film growth. For lower CH_4 additions, the film morphology depended upon the CH_4 concentration, with different gas mixing ratios producing microcrystalline diamond (MCD), NCD, or UNCD films. A two-dimensional computer model was used to calculate the gas phase composition for all these conditions at all positions within the reactor. Using the experimental and calculated data, we show that the observed film morphology can be rationalized using a model based on competition between H atoms, CH_3 radicals, and other C_1 species reacting with dangling bonds on the surface. The relative concentrations of each of these species close to the growing diamond surface determine the probability of a renucleation event occurring and hence the morphology of the subsequent film. This has been developed into a general mechanism for the deposition of MCD, NCD, and UNCD films from $Ar/CH_4/H_2$ gas mixtures which is consistent with published experimental observations. © *2006 American Institute of Physics*. [DOI: 10.1063/1.2214304]

I. INTRODUCTION

Diamond films can be deposited using a chemical vapor deposition (CVD) process involving the gas phase decomposition of a gas mixture containing a small quantity of a hydrocarbon in excess hydrogen.[1] A typical gas mixture uses $1\%CH_4$ in H_2, and this produces polycrystalline films with grain sizes in the microns or tens of micron range, depending upon growth conditions, substrate properties, and growth time. It is generally believed[2,3] that the main growth species in standard diamond CVD is the CH_3 radical, which adds to the diamond surface stepwise following successive hydrogen abstraction by H atoms. Thus, a high concentration of atomic H at the surface is a prerequisite for successful microcrystalline diamond (MCD) deposition. By increasing the ratio of methane in the standard CH_4/H_2 gas mixture from 1% to ~5%, the grain size of the films decreases and eventually becomes of the order of hundreds down to tens of nanometers. Such nanocrystalline diamond (NCD) films (often termed "cauliflower" or "ballas" diamond) are smoother than the microcrystalline ones, but have larger numbers of grain boundaries that contain substantial graphitic impurities. With further addition of CH_4, the films become graphitic.

Recently, so-called ultrananocrystalline diamond (UNCD) films have become a topic of great interest, since they offer the possibility of making smooth, hard coatings at relatively low deposition temperatures, which can be patterned to nanometer resolution.[4,5] These differ from NCD films, since they have much smaller grain sizes (~2–5 nm) and have little or no graphitic impurities at the grain boundaries. Most reports of the deposition of these films describe using a microwave (MW) plasma CVD reactor and gas mixture of $1\%CH_4$ in Ar, usually with addition of 1%–5% H_2. However, the fundamental growth mechanism of these UNCD films is still unclear. Originally it was suggested[6] that the C_2 radical played an important role in the growth mechanism. However, recent works by ourselves[7,8] and others[9] have cast doubt on the veracity of this C_2 mechanism. It now seems more likely that it is a delicate balance between the concentrations of a combination of predominantly C_1 hydrocarbon species close to the substrate surface that determines the growth morphology and hence the properties of the resulting film.

We have previously reported the use of similar $Ar/CH_4/H_2$ gas mixtures to deposit NCD (or UNCD) in a hot filament (HF) reactor,[10] with the compositional diagram for mixtures of Ar, CH_4, and H_2 being mapped out corresponding to the type of film grown (see Fig. 1). This broadly resembled the previous results of Lin *et al.*,[11] in that there is only a narrow composition range in which MCD or NCD is deposited. Generally, if the methane concentration becomes too high the filament became coated in a graphitic layer in-

[a)]Electronic mail: paul.may@bris.ac.uk

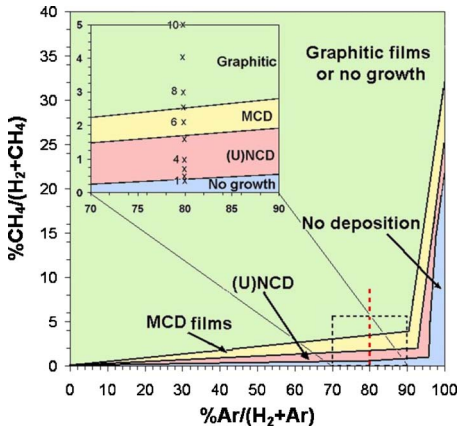

FIG. 1. (Color online) An experimental composition map of the $Ar/CH_4/H_2$ gas mixture for a hot filament reactor (adapted from Ref. 10). The positions of the boundary lines between the four regions were estimated from experimental data points. The upper region produced films that were predominantly sp^2 carbon in character (as determined by Raman spectroscopy) or caused the filament to become coated in a graphitic layer preventing film deposition. The region immediately below this produced MCD, giving a well resolved 1332 cm^{-1} Raman line and facetted crystallite sizes >0.1 μm. NCD or UNCD films (which appeared amorphous or had crystallite sizes <0.1 μm, but which also exhibited the 1332 and 1150–1190 cm^{-1} Raman lines) occurred only in a narrow region between those of MCD growth and no growth. The lower region is where no obvious films were deposited after 8 h of growth, although in some cases isolated crystallites were observed lying on top of the substrate. The inset is an enlargement of the area around 80% $Ar/(Ar+H_2)$ pertinent to the experiments in this paper. The crosses mark the data points and the adjacent number indicates the sample number as given in Table I.

hibiting gas activation and thus stopping subsequent film growth. Any films that are deposited under these conditions consist of graphitic or nondiamond carbon. With very low concentrations of methane, no film growth is seen (or the growth rate is too low to discern growth in a deposition time of 8 h). For the majority of the composition diagram, diamond films are deposited only in a very narrow region around $[CH_4]/([CH_4]+[H_2]) \sim 0.5\%-6\%$. The top boundary of this region is poorly defined, with the film quality gradually becoming more nanocrystalline with increasing CH_4 concentration until either the filament becomes covered in soot ending film growth or graphitic films are deposited. The lower boundary appears to be sharper, with the film quality changing from MCD to "no growth" within less than 1% change in CH_4 concentration. In the region of the MCD/no-growth boundary, we observed UNCD film deposition. The evidence that the films were UNCD was twofold. First, we observed the presence of the 1150–1190 cm^{-1} Raman line, which is believed[12] to originate from sp^2 carbon in *trans*-polyacetylene-like molecules trapped at the nanograin boundaries. Second, transmission electron microscopy (TEM) analysis revealed the films to be composed of randomly oriented crystals with grains <10 nm in size, with lattice spacings consistent with that of diamond. The growth rate of UNCD films in this boundary region was low, around 0.1 $\mu m\ h^{-1}$. Immediately below the boundary, i.e., just inside the no growth region, we often observed isolated nanoparticles lying on the surface, but which appeared not to be bonded to the surface.

In this paper we shall explore the chemistry occurring at these boundary regions in more detail. By fixing the $Ar/(Ar+H_2)$ ratio and varying the CH_4 concentration, we systematically studied the films produced as we traversed the boundaries between the various regions. As previously, we have also used two-dimensional modeling of the gas chemistry, including heat and mass transfer, in our hot filament reactors to attempt to understand the observations, and finally show how the experimental and theoretical data may help to shed some light on the UNCD growth mechanism.

II. EXPERIMENT

Films were deposited using a standard HF reactor operating at a pressure of 100 Torr using high purity Ar, CH_4, and H_2 as source gases. Mass flow controllers were used to control the ratios of the three gases. $[Ar]/([Ar]+[H_2])$ was kept constant at 80%, with the flow of CH_4 being varied to provide a range of values of $CH_4/(H_2+CH_4)$ crossing all the region boundaries, shown as a dashed line and as an insert in Fig. 1. The filament was made from 0.25 mm diameter Ta metal, wound around a 3 mm diameter core to produce a 2 cm long coil that was positioned 5 mm from the substrate surface. The filament temperature was kept constant at 2400 °C and monitored using a two-color optical pyrometer. The substrate was single crystal Si (100) which had been manually abraded prior to deposition using 1–3 μm diamond grit, and then ultrasonically cleaned with propan-2-ol. The substrate sat on a separate heater to give additional uniform heating and to maintain it at a temperature of ~850–900 °C (also measured using the optical pyrometer). Typical deposition times were 8 h, although some runs at higher methane concentrations were abandoned early due to premature filament breakage (due to the filament becoming covered with a thick graphitic coating, as mentioned previously).[10] After deposition the films were analyzed by UV (325 nm) laser Raman spectroscopy, and both scanning and transmission electron microscopies (SEM and TEM).

III. MODELING

In order to understand the gas phase chemistry occurring in the CVD chamber, the composition of the gas mixture was calculated using an existing two-dimensional (2D) model that has been specifically tailored to a reactor of this geometry.[13] The input parameters for the model were taken from the experimental values: pressure of 100 Torr, filament temperature of 2400 °C, and $Ar/H_2/CH_4$ gas flows as appropriate. The models comprise three blocks, which describe (i) activation of the reactive mixture (i.e., gas heating and catalytic H atom production at the filament surface), (ii) gas phase processes (heat and mass transfer and chemical kinetics), and (iii) gas-surface processes at the substrate. The gas phase chemistry and thermochemical input are taken from the GRI-MECH 3.0 detailed reaction mechanism for C/H/Ar gas mixtures.[14] As in previous studies[10,15–17] the conservation equations for mass, momentum, energy, and species concentrations, together with appropriate initial and boundary conditions, thermal and caloric equations of state, are each integrated numerically until steady-state conditions are attained. This yields spatial distributions of the gas temperature T_{gas},

the flow field, and the various species number densities and mole fractions. The incorporation of nine gas-surface reactions, involving H abstraction to form surface sites, and the subsequent reactions of these sites with H and hydrocarbon radicals, serves to alter significantly the gas composition close to the surface. The main effect of these reactions is to reduce the H atom concentrations directly above the growing diamond surface, which has major implications for subsequent growth. Note that the gas-surface reactions involve only those for which thermodynamic and kinetic data are available, i.e., those involving H, H_2, all the C_1H_x species, and C_2H_2. Since no data are available for the rates of reaction and their temperature dependence for C_2, C_2H, and higher hydrocarbon species reacting with diamond surface sites, these have not been included in the model. This means that the calculated concentrations close to the surface for these species may be overestimated.

IV. RESULTS

Table I shows the details for the experiments that were performed, as well as the description of the resulting film, if any. For $CH_4/(H_2+CH_4)$ concentrations less than that of sample 1 (0.32%) there was no observed deposition after 8 h. Sample 1 is at the boundary of the NCD/no-growth regions, and we see only very isolated nanoparticles scattered around the substrate surface (see Fig. 2), with no diamond Raman signal. Samples 2 and 3 lie within the UNCD region, but give nonuniform and noncontinuous NCD coatings, with growth rates and film coverage becoming less toward the edges of the film. Samples 4 and 5 also lie within this region but give continuous uniform coatings, as shown in Fig. 3(a). The Raman spectrum [Fig. 3(b)] shows evidence of a diamond line (1332 cm^{-1}), the *D* and *G* bands due to sp^2 carbon, as well as a feature between 1150 and 1190 cm^{-1} indicative of UNCD films. Sample 6 is in the MCD region [see Figs. 4(a) and 4(b)] and produces a continuous film of small facetted crystals, although the facets are poorly defined with rounded edges and corners. The growth rate is slow (<0.2 $\mu m\,h^{-1}$) compared to that for traditional $1\%CH_4/H_2$ gas chemistries ($0.5-1$ $\mu m\,h^{-1}$). As the methane concentration is increased, the crystal sizes decrease and become more rounded, until by sample 7, which is at the boundary of the MCD/graphitic growth region, the film is no longer continuous and is composed of isolated islands of microcrystals (see Fig. 5). Samples 8–10 are in the graphitic/no-growth region, and, here, the CH_4 concentration is so high that the filament became coated with a thick graphitic layer, reducing its efficiency preventing film growth.

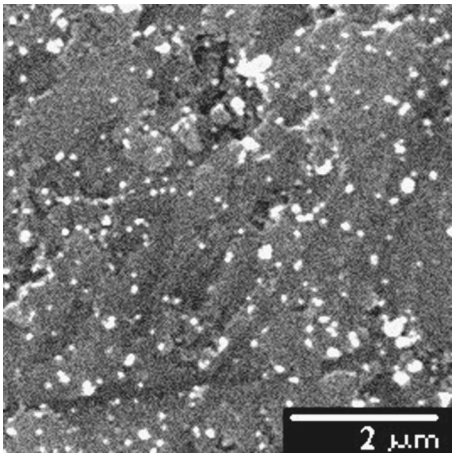

FIG. 2. SEM micrograph of sample 1, showing isolated nanoparticles (white) which are the beginnings of diamond nucleation.

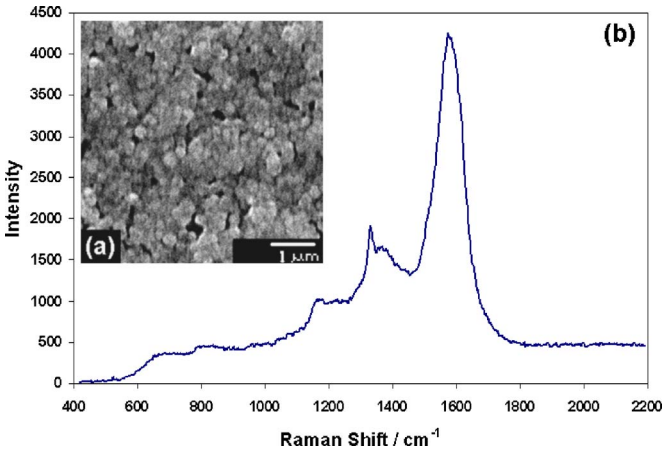

FIG. 3. (Color online) (a) SEM micrograph of sample 5, showing a NCD film composed of a layer of fused nanoparticles. (b) Raman spectrum of the film in (a) showing the broad *D* and *G* bands at 1370 and 1600 cm^{-1}, respectively, a sharp diamond peak at 1332 cm^{-1} and a peak at $\sim$1175 cm^{-1} characteristic of nanodiamond particles.

Modeling of the gas phase chemistry allows gas phase concentrations to be calculated as a function of axial *z* and radial *r* coordinates. Point ($z=0$, $r=0$) corresponds to the substrate center. The distance between the bottom of the hot filament and the substrate was $z\sim5$ mm, consistent with our experiments. An example is shown in Fig. 6 for CH_3 concentrations just above the substrate surface ($z=0.5$ mm), showing that the concentration remains roughly constant up to a

TABLE I. $CH_4/(CH_4+H_2)$ concentrations used in the deposition experiments, with $Ar/(Ar+H_2)$ constant at 80%.

Sample	$\%CH_4/(H_2+CH_4)$	Description of film
1	0.32	Isolated particles $<$100 nm diameter, widely scattered on surface.
2	0.48	0.25 μm diameter spherical nanoparticles, clustered together to form islands.
3	0.73	Spherical nanoparticles forming an almost continuous film.
4	1.02	Continuous UNCD film composed of densely packed, 100 nm diameter spheres. Spheres contain many fused nanodiamond crystals of grain size $<$10 nm.
5	1.46	Continuous UNCD film composed of densely packed, spherical balls, 0.25 μm diameter.
6	2.04	Continuous MCD film composed of small facetted crystals. Facets are poorly defined with rounded edges and corners.
7	2.48	Isolated $\sim$100 nm rounded microcrystals.
8	3.07	No film
9	3.94	No film
10	4.96	No film
11	5.99	No film

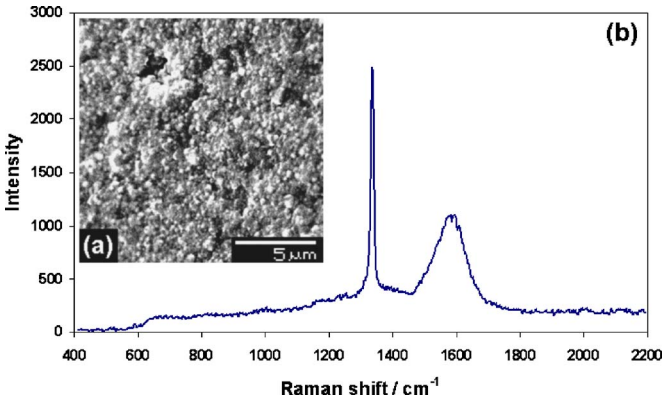

FIG. 4. (Color online) (a) SEM micrograph of sample 6, showing a MCD film with small rounded microcrystals. (b) Raman spectrum of the film in (a) showing the sharp diamond peak at 1332 cm^{-1} but a broad G band at 1600 cm^{-1}.

radius of ~6 mm from the center of the substrate (and hence the center of the filament), but drop off as r increases further. This is consistent with the across substrate uniformity seen in experiment; films generally had a uniform growth rate and appearance in the center of the Si substrate, but would have lower growth rates and worse quality towards the edges. This is one reason why we limited our substrate area to 1 cm^2.

Similar data are available for all of the major gas phase species, including C_2, H, H_2, C_2H, CH_2, CH, C atoms, etc. To compare with experimental observations, in this paper we shall use only the subset of data for (z=0.5 mm, r) (see Fig. 7), which corresponds to the position just above the Si substrate surface where the gas phase chemistry influences growth. From Fig. 7, we can see that over the range of CH_4 concentrations that produce the four different growth regions, the concentration of gas phase atomic H remains roughly constant at $\sim 2\times 10^{14}$ cm^{-3}. However, the CH_3 concentration drops by a factor of 25 on going from higher CH_4 gas mixtures to lower ones, while the atomic C concentrations increases by a factor of ~10. The concentration of C_2 is very low throughout, is $\sim 1\times 10^6$ times smaller than that of CH_3, and 1000 times smaller than that of atomic C. This is despite its concentration possibly being overestimated, as mentioned in Sec. III.

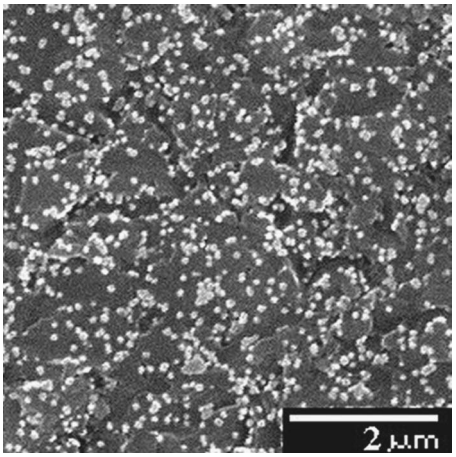

FIG. 5. SEM micrograph of sample 7, showing isolated, faceted particles with rounded edges and corners.

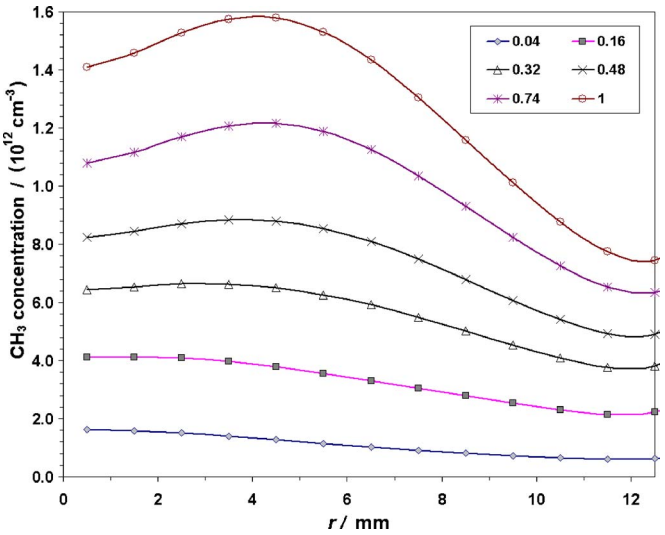

FIG. 6. (Color online) Radial profiles of calculated CH_3 concentrations just above the substrate (z=0.5 mm) for Ar/(Ar+H_2)=80% and different values of CH_4/(CH_4+H_2) percentage (from 0.04 to 1%) in the gas mixture, shown in the legend.

It is clear that the behavior of Ar/CH_4/H_2 gas mixtures in terms of diamond growth is significantly different from that of CH_4/H_2 gas mixtures, under similar process conditions. So the question is, what is the role of the argon? Is it simply an inert diluent, or does it affect the gas phase chemistry? Table II shows the calculated gas phase concentrations of selected species, both close to the substrate surface and close to the filament, for three different process gas mixtures/pressures: (i) standard 1%CH_4/H_2 at 20 Torr typical for MCD growth, (ii) 1%CH_4/H_2 at 100 Torr to ascertain the effect of the increased pressure, and (iii) Ar/H_2/CH_4 (80:20:0.2) at 100 Torr, as for the UNCD growth conditions of sample 4.

Comparing the columns in Table II for 1%CH_4/H_2 at the two different pressures close to the substrate surface, we see that most of the species concentrations do not change significantly with the increased pressure. The exceptions are

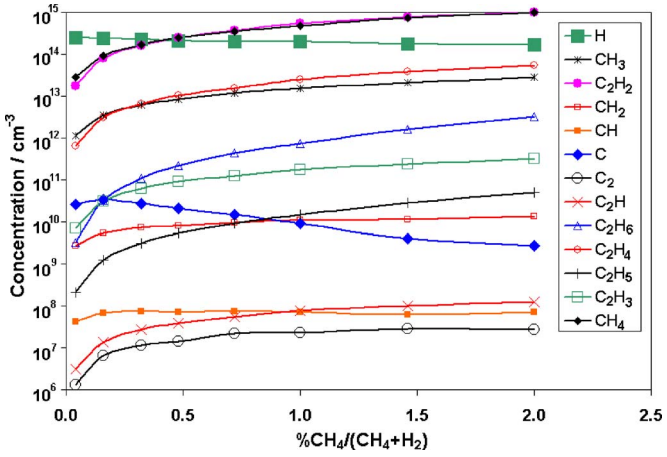

FIG. 7. (Color online) Calculated concentration for all the major gas phase species at (z=0.5 mm, r=0) for Ar/(Ar+H_2)=80% and different values of CH_4/(CH_4+H_2)) percentage in the gas mixture. Ar and H_2 have been excluded from this plot for clarity, but their concentrations remained almost constant over this range at $\sim 6\times 10^{17}$ and $\sim 2\times 10^{17}$ cm^{-3}, respectively.

TABLE II. Calculated gas temperature (T_{gas}) and selected species concentrations (in cm^{-3}) just above the substrate center and near the filament in our HFCVD reactor, for three gas mixtures and process pressures.

	Near substrate			Near filament		
	0.5 SCCM CH_4, 50 SCCM H_2, 20 Torr	2.5 SCCM CH_4 250 SCCM H_2, 100 Torr	0.5 SCCM CH_4, 50 SCCM H_2, 200 SCCM Ar, 100 Torr	0.5 SCCM CH_4, 50 SCCM H_2, 20 Torr	2.5 SCCM CH_4, 250 SCCM H_2, 100 Torr	0.5 SCCM CH_4, 50 SCCM H_2, 200 SCCM Ar, 100 Torr
T_{gas} (K)	1280	1280	1280	2220	2220	2220
H	4.66×10^{14}	5.38×10^{14}	5.13×10^{14}	2.86×10^{15}	1.18×10^{16}	1.50×10^{16}
CH_3	7.40×10^{13}	5.94×10^{13}	1.41×10^{13}	9.66×10^{13}	3.33×10^{14}	2.29×10^{13}
C_2H_2	2.03×10^{13}	7.86×10^{14}	6.76×10^{14}	1.10×10^{13}	4.82×10^{14}	4.96×10^{14}
CH_2	1.96×10^{11}	2.67×10^{10}	5.59×10^{10}	3.61×10^{12}	1.33×10^{13}	3.95×10^{12}
CH	3.27×10^{9}	1.02×10^{8}	1.15×10^{9}	3.85×10^{11}	1.10×10^{12}	1.62×10^{12}
C	4.75×10^{10}	1.06×10^{9}	2.39×10^{11}	6.51×10^{11}	1.81×10^{12}	1.27×10^{13}
C_2	2.21×10^{9}	2.17×10^{9}	1.41×10^{9}	2.44×10^{9}	3.40×10^{10}	4.47×10^{11}
$C_2(X)$	3.97×10^{6}	2.82×10^{6}	8.20×10^{7}	2.80×10^{7}	7.82×10^{8}	3.78×10^{10}
C_2H	1.93×10^{7}	1.58×10^{8}	5.26×10^{8}	1.11×10^{10}	4.01×10^{11}	1.90×10^{12}
C_2H_6	8.30×10^{11}	2.79×10^{12}	1.23×10^{11}	7.01×10^{9}	2.57×10^{10}	5.05×10^{7}
C_2H_4	7.63×10^{12}	5.63×10^{13}	1.15×10^{13}	1.68×10^{12}	4.37×10^{12}	4.69×10^{10}
C_2H_5	2.54×10^{10}	6.26×10^{10}	4.68×10^{9}	2.12×10^{10}	6.07×10^{10}	2.51×10^{8}
C_2H_3	1.03×10^{11}	2.62×10^{11}	2.77×10^{11}	3.20×10^{11}	7.52×10^{11}	4.09×10^{10}
CH_4	5.96×10^{14}	3.08×10^{15}	1.79×10^{14}	1.72×10^{14}	6.29×10^{14}	9.56×10^{12}
H_2	1.50×10^{17}	7.51×10^{17}	1.91×10^{17}	8.39×10^{16}	4.22×10^{17}	1.17×10^{17}
Ar	⋯		5.64×10^{17}	⋯		3.05×10^{17}
H/CH_3	6.3	9.1	36.4	29.2	35.4	655
CH_3/C	1560	1251	59	148	184	1.80

C_2H and C_2H_2 which have increased in concentration by 10–20 times at higher pressures, whereas all the reactive C_1 radicals (except CH_3) have decreased by around a factor of 10. Near the filament the concentrations of all the reactive species (except H) have increased. So it appears that the effect of increasing the pressure from 20 to 100 Torr is to localize the gas reactions closer to the filament, with the gas composition further from the filament evolving toward that of the more stable species. However, since thermal and diffusive transport through a mainly H_2 gas mixture is relatively high, these effects are minimal, and there is still sufficient atomic H and CH_3 close to the substrate to grow MCD at high rates.

This situation is enhanced, however, when the gas mixture is mainly Ar, since this has much poorer thermal and diffusive transport. Near the filament the concentration of CH_4 is reduced by a factor ~20, indicating a much higher degree of dissociation of methane, producing less CH_3 but more CH_2, CH, and especially atomic C. This distribution of reactive species rapidly cools away from the filament, and reacts to form more stable species, but even close to the substrate surface there is still sufficient H and CH_3 to initiate diamond growth. The important difference is in the concentration of atomic C reaching the substrate. Because ~20 times as much atomic C was created at the filament in the Ar-containing plasma at 100 Torr compared to the CH_4/H_2 plasma at 20 Torr, five times as much C survives to reach the substrate where it can affect the nature of the growth. This idea is further illustrated by the ratios given in Table II for H/CH_3 and CH_3/C. Close to the substrate, the ratio of H/CH_3 is high for all gas mixtures, allowing H abstraction reactions to dominate the gas-surface chemistry. However, the ratios of CH_3/C decrease from values >1000 in the H_2-rich gas mixtures to ~59 in the Ar-containing mixture. This suggests that in the Ar-containing mixtures, atomic C may become a significant competitor to CH_3 for gas-surface addition reactions.

V. DISCUSSION

In our previous paper[8] we proposed that the growth rates of MCD, NCD, and UNCD can be modeled assuming that the growth process occurs via H abstraction reactions on the diamond substrate followed by addition of *only* C_1 species (including CH_3, CH_2, CH, and C atoms). We assumed that since C_2 species are present in the gas phase above the substrate in much lower concentrations, they will probably play only a minor role in growth. Depending upon which C_1 species adds to the substrate, there are different rate laws (with correspondingly different rate constants) which govern the kinetics and hence the growth rate. It is possible to estimate the contribution to the growth rate G (in $\mu m\,h^{-1}$) of the important C_1 species, using formulas derived in Ref. 18,

$$G_{CH_3} = 3.8\times10^{-14}T_{ns}^{0.5}[CH_3]R^2, \quad (1)$$

$$G_{CH_x} = 3.9\times10^{-14}T_{ns}^{0.5}[CH_x]R, \quad (2)$$

where T_{ns} is the gas temperature near the substrate (obtained from the modeling results) and CH_x is for $x=0,1,2$. R is the fraction of open carbon sites given by $R=C_d/(C_d+C_dH)$,

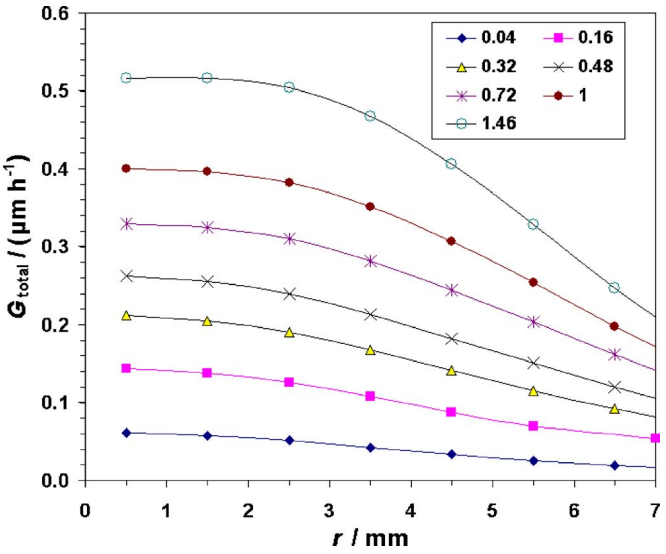

FIG. 8. (Color online) Radial profile of calculated total growth rates from all C_1 species for $Ar/(Ar+H_2)=80\%$ and different values of $CH_4/(CH_4+H_2)$ percentage in the gas mixture from 0.04% to 1.46%.

where C_d and C_dH are the respective densities of open- and hydrogen-terminated diamond surface sites. This fraction R mainly depends on the rate constants for the surface H abstraction and addition reactions and can be calculated using the data and following the procedure outlined in our previous paper.[8] For example,

$$R = 1/\{1 + 0.3\exp(3430/T_s) + 0.1\exp(-4420/T_s) \times [H_2]/[H]\}. \quad (3)$$

Here T_s is the substrate temperature in Kelvin, and [H] and $[H_2]$ are the atomic and molecular hydrogen concentrations near the substrate. An example of the calculated growth rates using this method is shown in Fig. 8. The predicted growth rates and radial profiles are very close to those observed in experiment, except at the higher methane concentrations, where the model does not predict the falloff in growth due to the filament poisoning effects mentioned earlier.

Since the model can differentiate between growth from CH_3 radicals and growth from other C_1 species, it is informative to plot the percentage of the total growth that is due to CH_3 as a function of methane concentration. This is shown in Fig. 9 as a function of radial distance from the center of the substrate r and in Fig. 10 for $r=0$ and $z=0.5$ mm (i.e., just above the center of the growing substrate surface). It is clear from these figures that for CH_4 concentrations greater than about $CH_4/(CH_4+H_2)=0.5\%$, the growth is due almost entirely to CH_3 species adding to the diamond surface. However, below this value, although the total growth rate is dropping, other C_1 species (especially C atoms and CH radicals) begin to make a significant contribution to the growth rate. Thus, the modeling predicts a switch in growth mechanism from CH_3-dominated growth at high CH_4 concentrations to multiple-C_1-species growth at lower CH_4 concentrations.

In order to check that these ideas are of general significance, we have used the same simulation procedure with published data for a different hot filament CVD system from

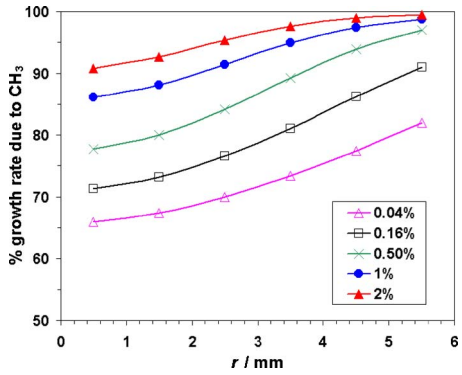

FIG. 9. (Color online) Plot of calculated percentage growth rate due to CH_3 compared to that from all C_1 species (i.e., $100\times G_{CH_3}/G_{total}$) at different radial coordinates for $Ar/(Ar+H_2)=80\%$ and different values of $CH_4/(CH_4+H_2)$ percentage in the gas mixture.

the Erlangen-Nurnberg University group.[19] For their growth conditions, a $1\%CH_4/H_2$ mixture for various gas pressures shows an even more significant contribution by C atoms to the total growth rate, as seen from Fig. 11, especially at lower pressures. Moreover, as the process pressure decreases below 14 Torr the films became NCD/UNCD in nature, and this is mirrored by a corresponding increase in the contribution of C_1 species to the growth.

Using these data, we can now begin to rationalize the different observed experimental growth regions with the gas phase chemistry experienced by the surface in each case, and this is summarized in the flowchart in Fig. 12. In order to grow diamond of any type, the concentration of atomic H above the substrate must be large, since H atoms are necessary to drive all the H abstraction reactions and the subsequent chemical processes. As mentioned previously,[8] the ratio of $[H]:[CH_3]$ just above the substrate is an indicator for the type of film that can be grown, for the HF system used here with $Ar/H_2/CH_4$ gas mixtures.

(i) When $[H]:[CH_3]$ falls below a value of ~5, then there are insufficient H atoms to initiate the processes responsible for successful diamond growth. The hydrocarbon species therefore react at either the film surface or at the filament surface to produce graphitic films.

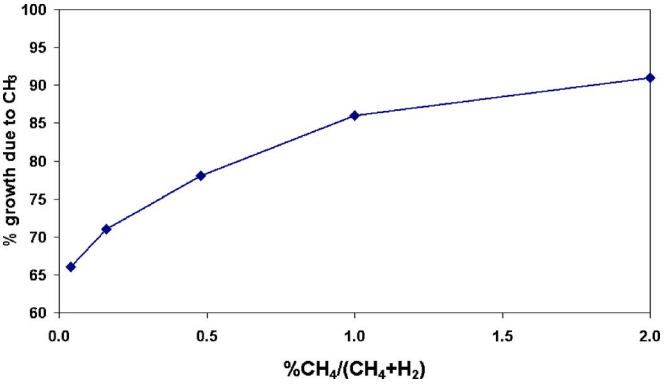

FIG. 10. (Color online) Plot of calculated percentage growth rate due to CH_3 compared to that from all C_1 species (i.e., $100\times G_{CH_3}/G_{total}$) at the center of the substrate ($r=0$) for $Ar/(Ar+H_2)=80\%$ and different values of $CH_4/(CH_4+H_2)$ percentage in the gas mixture.

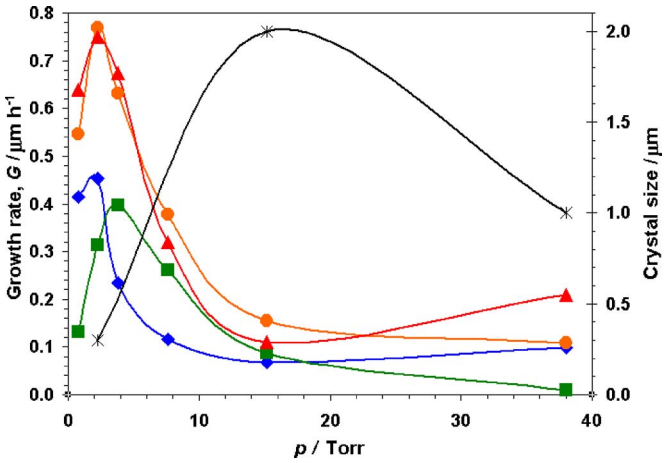

FIG. 11. (Color online) Experimental measurements of crystal size (×) and growth rate (▲), along with our simulation of the growth rate (●) as a function of process pressure p for the diamond growth conditions published in Ref. 19. Also shown is the growth rate due to CH_3 (♦) and that due to the total of the other C_1 species (■), both calculated using Eqs. (1) and (2). The Raman spectra in Ref. 19 show that the film quality improved as the pressure was reduced from 40 to 14 Torr, but then the grain size rapidly decreased until by 2 Torr the films had become smooth and nanocrystalline, with the Raman spectra showing the 1170 cm^{-1} peak characteristic of UNCD.

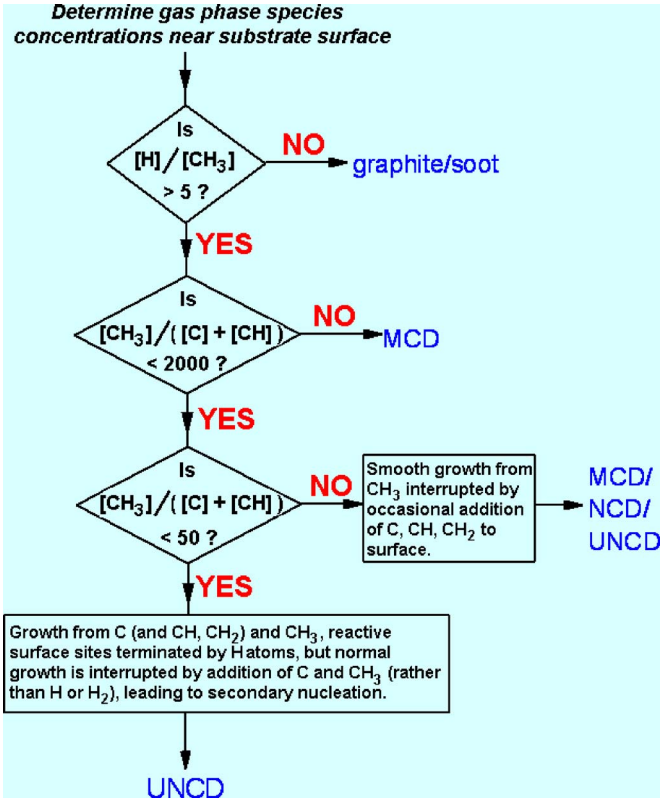

FIG. 12. (Color online) Flowchart for the model of diamond growth which predicts which type of film is deposited.

(ii) For $[H]:[CH_3]>5$ there is sufficient H to initiate diamond growth, and the growth mechanism then depends upon the ratio of methyl concentration to that of the total of the other C_1 species, i.e., $[CH_3]:([C]+[CH]+[CH_2])$, although CH_2 can be ignored as it contributes an insignificant amount to the growth rate. Therefore, for $[CH_3]:([C]+[CH])>\sim 2000$, the CH_3 concentration is so large relative to the other C_1 species that all the surface addition reactions are dominated by CH_3. Hence, this methyl-dominated growth mechanism gives rise to faceted MCD films, just as it would in traditional $1\%CH_4/H_2$ gas mixtures. However, the lower absolute concentration of CH_3 means that the growth rates are much reduced over those seen in $1\%CH_4/H_2$ gas mixtures.

(iii) If $[H]:[CH_3]$ remains greater than ~5, but with lower CH_4 added to the gas mixture, $[CH_3]:([C]+[CH])$ becomes less than ~2000, and the probabilities that other C_1 species add to the growing diamond surface become significant compared to that of CH_3. For CH_3 addition, the surface "dangling bond" is terminated, and the diamond growth cannot proceed further until one of the adjacent H's is removed by a H abstraction reaction.[20] But if a C atom adds to the surface, one dangling bond is satisfied, but two or three new dangling bonds are created. These provide the opportunity for addition of other C_1 species in an orientation that does not necessarily propagate the symmetry of the diamond lattice. In other words, this creates a potential renucleation site. With increasing renucleation, the grain size becomes smaller and the film morphology changes from MCD to NCD, and eventually to UNCD.

(iv) With even lower CH_4 in the gas mixture, the ratio $[CH_3]:([C]+[CH])$ becomes less than ~50. At this point, the growth rates from the other C_1 species become similar to that from CH_3 (see Fig. 9). The H concentration is still sufficient to terminate most of the reactive surface sites, but frequent addition of C_1 species to some sites instead results in a net higher rate of renucleation. Hence, we now get predominantly UNCD.

(v) With yet lower CH_4 in the gas mixture, the concentrations of gas phase C_1 species now become so low that the overall diamond growth rate is negligible, and no deposition is observed in reasonable time scales.

(vi) The role of the Ar in the gas mixture appears to reduce diffusion transfer (diffusion coefficients drop with total gas concentration) and thus to increase atomic hydrogen concentration near the filament. This is because in HFCVD reactors the concentration of atomic hydrogen near the filament is determined by a balance between catalytic H_2 dissociation at the filament surface and H atom diffusion transfer from the near-filament region to the whole reactor. As a result, the degree of dissociation of the CH_4 is increased with Ar addition, thereby creating a very high concentration of C_1 species (especially atomic C) close to the filament. Since Ar is chemically inert, more of these C_1 species survive to reach the diamond surface, where they compete for surface reaction sites with CH_3. This would also be broadly true for MW plasma systems, where the Ar reduces thermal conductivity and increases the local plasma temperature, and thus increases the degree of CH_4 dissociation leading to a

high $C:CH_3$ ratio at the substrate surface.[8]

(vii) For standard MCD growth conditions, where there are relatively high concentrations of H and much lower concentrations of C, CH, etc., the appearance of a C atom with free dangling bonds on the surface could be created as a result of two successive H atom abstractions from a CH_2 surface group. This event, with a probability proportional to R^2, could be the necessary prerequisite for renucleation during normal MCD growth, and thus would be a criterion for determining the crystal size obtained. Generally, the average crystal size will be inversely proportional to some sum of R^2 and $([C]+[CH])/(\Sigma[CH_x])$, $x=0-3$. This idea will be discussed in future papers.

It should be noted that the mechanism of UNCD/NCD/MCD growth outlined in (i)–(vii), above, and the growth rate expressions (1) and (2) are in good agreement with our own experimental data shown here (and our data for MW UNCD deposition in Ref. 8) and the experimental data[19] of the Erlangen-Nurnberg University group for average crystal sizes and growth rates as function of gas pressure (Fig. 10). Furthermore, this mechanism is consistent with many of the other experimental observations concerning UNCD growth in the literature.

(i) The species which we presume to be responsible for UNCD growth and renucleation (i.e., CH_3, CH_2, CH, and C atoms) are present in sufficient quantities near the surface to account for the observed (low) growth rates of UNCD.

(ii) The mechanism is not specific to reactor types or geometries, consistent with the observation that UNCD can be deposited in HF and MW reactors.

(iii) The random nature of the renucleation is consistent with the roughly spherical nature of UNCD grains.

(iv) The small grain size is accounted for by the high probability of renucleation as the H concentration decreases. With increasing H_2 additions, CH_3 growth dominates and the grain size increase towards that of MCD, as seen experimentally.[21,22]

(v) The variation of gas phase concentrations of CH_3 and the other C_1 species from the center of the filament explains observed nonuniformities in film thickness across the substrate. Small local variations in the ratio of these growth precursors caused by inhomogeneities in the orientation of the filament and in the gas mixing (especially in large reactors) would have a large effect upon the local growth conditions. Some areas of the film would experience predominantly CH_3 growth and be more microcrystalline, while other would experience CH_3+CH_x growth and be UNCD. This is consistent with the observation that MCD and UNCD can be deposited simultaneously.[23]

(vi) The abrupt grain boundaries containing little or no sp^2 carbon are consistent with the idea that the predominant growth will be that of diamond. Due to the high concentration of H atoms near the surface, most surface sp^2 carbon sites will be rapidly hydrogenated to sp^3, except for the relatively rare occurrence where the site forms a defect leading to renucleation. Thus, there is no mechanism for generating large amounts of sp^2 C. The only sp^2 C present will be that which is created at the grain boundary due to mismatches in the neighboring grain lattice directions.

(vii) The proposed mechanism is consistent with the observation that UNCD films can be grown without the need for seeding by nanocrystals (although seeding helps) and even on single crystal diamond surfaces.

(viii) UNCD can be deposited in MW CVD reactors at temperatures as low as ~400 °C with only slightly lower growth rates and without marked change in structure.[5] This can be explained since a growth mechanism incorporating addition of highly reactive C atoms to the surface will have a much different, and *lower*, activation barrier than one involving purely CH_3. As seen from Eqs. (1)–(3), the activation barrier for C addition is two times lower than for CH_3. Another necessary condition for successful UNCD growth at low substrate temperatures is to retain high concentrations of C and H atoms near the growing surface. In MW reactors this is realized due to the hot plasma being in close vicinity to the substrate.

(ix) The calculated concentrations of both C_2 (1.4×10^9 cm^{-3}) and C_2H (5.3×10^8 cm^{-3}) close to the substrate surface in the HF reactor are extremely low compared to both that of CH_3 (1.4×10^{13} cm^{-3}) and the other C_1 species (e.g., $\sim10^{11}$ cm^{-3} for atomic C). This shows that neither C_2 nor C_2H can play an important role in the growth of UNCD. However, for MW plasmas that deposit UNCD, the concentrations for C_2 and C_2H are calculated[8] to be much higher ($[C_2]\sim10^{11}$ cm^{-3}, $[C_2H]\sim10^{12}$ cm^{-3}, with $[CH_3]\sim10^{13}$ cm^{-3}) than in the hot filament reactor presented here. This is due to the different temperature distributions in the two reactors, with MW reactors having a much higher gas temperature closer to the substrate surface than HF reactors.[10] C_2 and C_2H are only found in the hot regions, since they rapidly react to form more stable species (e.g., C_2H_2) at lower gas temperature. The high concentration of these two species in MW reactors originally led to the suggestion that one or both of them might be responsible for UNCD growth or renucleation. However, the fact that UNCD can be grown in both HF and MW systems shows that UNCD growth is independent of the gas phase concentration of C_2 or C_2H and is instead determined by the relative concentrations of the C_1 species.

VI. CONCLUSIONS

In this paper we have tried to understand the growth mechanisms of the various forms of diamond film produced in a HF reactor using $Ar/H_2/CH_4$ gas mixtures. We have shown that the observed film morphology and characteristics can be rationalized using a model based on competition to react with dangling bonds on the surface by H atoms, CH_3

radicals, and other C_1 species. Renucleation occurs as two successive events—adsorption of a C atom (or CH_x, $x<2$) on a free radical surface site, $C(s)$,

$$C(g) + C(s) \rightarrow C - C(s),$$

followed either by (i) reaction with other gas phase hydrocarbon radicals CH_x rather than with H or H_2 or by (ii) restructuring of the surface. Either process results in a stable surface defect which would halt the normal stepwise growth of diamond and act as a renucleation site. For the typical conditions used to deposit MCD/NCD and UNCD in a variety of different diamond CVD reactors (including MW and HF CVD reactors), the reactions with hydrogen which lead to continuous normal diamond growth are much more frequent events than the reactions with CH_x or surface reconstruction. Thus propagation of the diamond lattice occurs more often than the rarer addition of CH_x which can lead to renucleation. But depending upon the gas mixture and reaction conditions used, the relative concentrations of each of these species close to the growing diamond surface (e.g., H/CH_3, $(C+CH)/CH_3$, $(H+H_2)/\Sigma CH_x$) determine the probability of a renucleation event occurring, and hence the morphology of the subsequent film, be it MCD, NCD, or UNCD. C_2 and C_2H are in too low a concentration close to the substrate surface to be important in either the growth or renucleation steps and may be considered to be "spectator" molecules.

ACKNOWLEDGMENTS

The authors would like to thank Professor Mike Ashfold, Edward Crichton, and other members of the Bristol diamond group for useful discussions. One of the authors (Yu.A.M.) wishes to thank Russian FSSTP Contract No. 02.445.117201 and ISTC Grant No. 2968/2005. They also wish to thank Sean Davis and other members of the Bristol EM laboratory for TEM analysis.

[1] P. W. May, Philos. Trans. R. Soc. London, Ser. A **358**, 473 (2000).
[2] S. J. Harris, Appl. Phys. Lett. **56**, 2298 (1990).
[3] D. G. Goodwin and J. E. Butler, in *Handbook of Industrial Diamonds and Diamond Films*, edited by M. A. Prelas, G. Popovici, and L. K. Bigelow (Dekker, New York, 1998).
[4] *Synthesis, Properties and Applications of Ultrananocrystalline Diamond*, NATO Science Series II: Mathematics, Physics and Chemisrty, Vol. 192, edited by D. M. Gruen, O. A. Shenderova, and A. Ya. Vul' (Springer, New York, 2005), pt. II, Vol. 192.
[5] X. Xiao, J. Birrell, J. E. Gerbi, O. Auciello, and J. A. Carlisle, J. Appl. Phys. **96**, 2232 (2004).
[6] D. Zhou, T. G. McCauley, L. C. Qin, A. R. Krauss, and D. M. Gruen, J. Appl. Phys. **83**, 540 (1998).
[7] E. Crichton and P. W. May, presented at ICNDST-9, Tokyo, April 2004 (unpublished); presented at Diamond 2004, Italy (unpublished).
[8] P. W. May, Yu. A. Mankelevich, J. N. Harvey, and J. A. Smith, J. Appl. Phys. **99**, 104907 (2006).
[9] J. R. Rabeau, P. John, J. I. B. Wilson, and Y. Fan, J. Appl. Phys. **96**, 6724 (2004).
[10] P. W. May, J. A. Smith, and Yu. A. Mankelevich, Diamond Relat. Mater. **15**, 345 (2006).
[11] T. Lin, G. Y. Yu, A. T. S. Wee, and Z. X. Shen, Appl. Phys. Lett. **77**, 2692 (2000).
[12] A. C. Ferrari and J. Robertson, Phys. Rev. B **63**, 121405 (2001).
[13] Y. A. Mankelevich, A. T. Rakhimov, and N. V. Suetin, Diamond Relat. Mater. **7**, 1133 (1998).
[14] G. P. Smith *et al.*, http://www.me.berkeley.edu/gri-mech/
[15] Y. A. Mankelevich, N. V. Suetin, M. N. R. Ashfold, J. A. Smith, and E. Cameron, Diamond Relat. Mater. **10**, 364 (2001).
[16] M. N. R. Ashfold, P. W. May, J. R. Petherbridge, K. N. Rosser, J. A. Smith, Y. A. Mankelevich, and N. V. Suetin, Phys. Chem. Chem. Phys. **3**, 3471 (2001).
[17] J. A. Smith, J. B. Wills, H. S. Moores, A. J. Orr-Ewing, Yu. A. Mankelevich, and N. V. Suetin, J. Appl. Phys. **92**, 672 (2002).
[18] Y. A. Mankelevich, N. V. Suetin, M. N. R. Ashfold, W. E. Boxford, A. J. Orr-Ewing, J. A. Smith, and J. B. Wills, Diamond Relat. Mater. **12**, 383 (2003).
[19] S. Schwarz, S. M. Rosiwal, M. Frank, D. Breidt, and R. F. Singer, Diamond Relat. Mater. **11**, 589 (2002).
[20] S. Skokov, B. Weiner, and M. Frenklach, J. Phys. Chem. **98**, 7073 (1994).
[21] J. Birrell, J. E. Gerbi, O. Auciello, J. M. Gibson, J. Johnson, and J. A. Carlisle, Diamond Relat. Mater. **14**, 86 (2005).
[22] D. Zhou, D. M. Gruen, L. C. Qin, T. G. McCauley, and A. R. Krauss, J. Appl. Phys. **84**, 1981 (1998).
[23] Y. K. Liu, Y. Tzeng, C. Liu, P. Tso, and I. N. Lin, Diamond Relat. Mater. **13**, 1859 (2004).